J. Fluid Mech. (2011), *vol.* 679, *pp.* 194–218.
doi:10.1017/jfm.2011.131

Sound generation by laminar premixed flame annihilation

MOHSEN TALEI[1], MICHAEL J. BREAR[1]† AND EVATT R. HAWKES[2]

[1]Department of Mechanical Engineering, University of Melbourne, Victoria 3010, Australia
[2]School of Photovoltaic and Renewable Energy Engineering/School of Mechanical and Manufacturing Engineering, University of New South Wales, Sydney NSW 2052, Australia

(Received 11 June 2010; revised 24 February 2011; accepted 10 March 2011; first published online 18 April 2011)

This paper presents a numerical and theoretical investigation of the sound generated by premixed flame annihilation. Planar, axisymmetric and spherically symmetric flame annihilation events are considered. The compressible Navier–Stokes, energy and progress variable equations are first solved using simple chemistry simulations, resolving both the flame dynamics and the acoustics. These simulations show that the amplitude of the far-field sound produced by the annihilation events depends on the flame thickness, particularly for the axisymmetric and spherically symmetric flame annihilation events. The flame propagation velocity is also always observed to increase significantly prior to flame annihilation, which is in keeping with other reported experimental and numerical studies. A theory is then presented that relates the far-field sound to the flame annihilation event by using a previously reported and extended form of Lighthill's acoustic analogy. A comparison with the numerical results shows that this theory accurately represents the far-field sound produced by considering only the temporal heat release source term in Lighthill's acoustic analogy, as reported by others. Additional assumptions of an infinitely thin flame and constant flame speed are then invoked in an attempt to simplify the problem. In the planar annihilation, this theory results in good predictions of the overall pressure change. However, these assumptions lead to significant under-prediction of the amplitude of far-field sound produced for the axisymmetric and spherically symmetric annihilation events. Finally, dimensional reasoning supported by the simulations and theory is used to develop scalings of the far-field sound in terms of the flame parameters.

Key words: aeroacoustics, combustion

1. Introduction

Combustion is a significant source of noise pollution. Combustion generated sound also plays a central role in the stability of many engineering devices, such as industrial burners, gas turbines and rockets (e.g. Lieuwen 2003; Lieuwen & Yang 2006; Candel *et al.* 2009; Schwarz & Janicka 2009). The ongoing pursuit of quieter and cleaner combustion in these devices provides a continued need for further refinements in our understanding of combustion generated sound. As a result, experimental, theoretical and numerical studies of this phenomenon appear regularly in the literature.

† Email address for correspondence: mjbrear@unimelb.edu.au

The first studies of combustion generated sound were undertaken when the fundamental theories of both combustion and sound generation were experiencing rapid development. Smith & Kilham (1963) studied sound generation by open, premixed turbulent flames. This work appears to be the first to report experimentally that sound generation by a *turbulent* premixed flame can be essentially monopolar, but the work only briefly discussed why this might be the case. Nonetheless, this is a remarkable result given the highly non-uniform nature of turbulent flows and is in distinct contrast to the sound produced by non-reacting, turbulent jets. The theory of Bragg (1963) also assumed that combustion generated sound is monopolar, but this appears to be based on physical reasoning rather than observation.

Thomas & Williams (1966) constructed a theory describing sound generation by changes in the volume of a premixed laminar flame. This theory could only accommodate monopolar sound sources since the geometry considered was spherically symmetric. Thomas & Williams (1966) compared this theory to measurements of the sound radiated from a premixed gas mixture confined within soap bubbles and achieved good agreement when the gas bubble was centrally ignited. Hurle *et al.* (1968) extended this simple theory to investigate the sound produced by open, turbulent premixed flames, and again found reasonable agreement with experiment. These two studies provided evidence that the mechanism of sound generation by laminar and turbulent flames can be closely related.

Strahle (1971) then extended Lighthill's acoustic analogy (Lighthill 1951) to combusting flows. Since Lighthill's analogy is derived from the equations of fluid motion, Strahle's work was able to argue from a more fundamental basis that monopolar sound sources can indeed appear in turbulent combusting flows. Several later works have since also based their arguments on extensions of Lighthill's and other acoustic analogies (e.g. Hassan 1974; Kotake 1975; Strahle 1978; Dowling 1992; Lieuwen, Mohan & Rajaram 2006). Under the assumptions of low Mach number and a constant average mixture molecular weight, Lighthill's acoustic analogy can be simplified to an inhomogeneous wave equation with a single monopolar source term (Strahle 1978; Dowling 1992; Truffaut, Searby & Boyer 1998). This source term has been written in terms of time derivatives of the heat release rate or the flame volume. Relating these quantities to the flame motion then allows a relation for the far-field sound to be obtained. Much of the subsequent theoretical work on this problem starts from this premise and continues to yield useful insights (e.g. Strahle 1985; Clavin & Siggia 1991; Dowling 1992; Howe 1998; Schuller, Durox & Candel 2002; Lieuwen & Yang 2006; Hirsch *et al.* 2007).

One mechanism affecting the flame volume, and hence sound generation, is flame annihilation (Kidin *et al.* 1984, 1988; Candel, Durox & Schuller 2004). These annihilation events have been observed in highly corrugated flames (Candel *et al.* 1990) including acoustically excited laminar (e.g. Durox *et al.* 2009; Karimi *et al.* 2009) and turbulent flames (Balachandran *et al.* 2005). When two flame surfaces interact the unburnt gas trapped between these surfaces is consumed, resulting in a rapid reduction in flame surface area and thus heat release. Kidin *et al.* (1984) examined the noise generated by an excited conical flame with a speaker at the base. They observed two peaks in the pressure history in the far-field. The first peak was largest and was attributed to the collapse of a 'flame neck', and the second one was attributed to the consumption of a 'pocket' of unburnt gas produced by the first collapse.

Candel *et al.* (2004) studied sound generation in three configurations: flame interaction with a cold plate, mutual flame annihilation and vortex flame interaction.

Since the maximum rate of decrease in the flame surface area and hence heat release rate determined the pressure amplitude in these three cases, Candel *et al.* (2004) concluded that the dominant mechanism of sound generation was flame surface destruction. They then suggested that flame surface destruction is a dominant source of sound in turbulent combustors.

Several numerical studies have examined flame annihilation in detail without considering sound production (e.g. Chen & Sohrab 1995; Echekki, Chen & Gran 1996; Wichman & Vance 1997; Petrov & Ghoniem 1998; Sun & Law 1998; Lu & Ghosal 2003). The dynamics of converging spherical and cylindrical flames have also been investigated both experimentally and numerically (e.g. Sivashinsky 1974; Bradley, Gaskell & Gu 1996; Durox, Ducruix & Candel 2001; Baillot, Durox & Demare 2002; Pantano & Pullin 2003; Lu & Ghosal 2004). Thus, if sound generation by flame annihilation is a significant sound source, these non-acoustic studies may provide insights into the problem.

Sound generation by combustion has been studied using large eddy simulation (LES) (e.g. Bui *et al.* 2005; Birbaud *et al.* 2006; Ihme, Bodony & Pitsch 2006; Flemming, Sadiki & Janicka 2007; Bui, Schröder & Meinke 2008; Ihme, Pitsch & Bodony 2009) and direct numerical simulations (DNS) (e.g. Miyauchi, Tanahashi & Li 2001; Zhao & Frankel 2001; Tanahashi *et al.* 2002; Laverdant & Thévenin 2003, 2005; Shalaby, Laverdant & Thévenin 2009; Najafi-Yazdi, Lew & Mongeau 2010). Since all relevant flow physics should be resolved in DNS, it offers the potential of further insight into the sound generation problem.

The aims of this study are twofold. First, this study will investigate the mechanism of sound generation in three premixed flame configurations using simple chemistry simulations resolving both the flame dynamics and the acoustics. Simple chemistry is used since the dependence of radiated sound on even basic parameters such as the flame thickness is not yet established. A theory is then developed for these three configurations using an extended form of Lighthill's equation (Dowling 1992). Key parameters are subsequently identified and their influence on the far-field sound is investigated further. The three configurations studied are:

(i) a planar case, in which two flat flames propagate towards each other until they annihilate;

(ii) an axisymmetric flame, which propagates inwards and then self-annihilates; and

(iii) a spherically symmetric flame, which propagates inwards and self-annihilates.

Any three-dimensional flame annihilation event can be approximated by at least one of these canonical configurations. For example, the collapse of the 'flame neck' and consumption of the flame 'pocket' reported by Kidin *et al.* (1984) can be modelled as axisymmetric and spherically symmetric annihilation events, respectively. As such, it is hoped that both the simulations and the theory will yield results that are useful in understanding combustion generated sound more generally.

2. Governing equations

For an irreversible single step reaction, the governing equations in a one-dimensional domain with spatial coordinate ζ may be expressed as follows:

$$\frac{\partial \rho}{\partial t} + \frac{1}{\zeta^n}\frac{\partial \zeta^n \rho u}{\partial \zeta} = 0, \tag{2.1}$$

$$\frac{\partial \rho u}{\partial t} + \frac{1}{\zeta^n}\frac{\partial \zeta^n \rho u^2}{\partial \zeta} + \frac{\partial p}{\partial \zeta} = \frac{1}{\zeta^n}\frac{\partial \zeta^n \tau_{\zeta\zeta}}{\partial \zeta} - n\tau_{\phi\phi}/\zeta, \tag{2.2}$$

$$\frac{\partial \rho e_t}{\partial t} + \frac{1}{\zeta^n}\frac{\partial}{\partial \zeta}[\zeta^n(\rho e_t + p)u] = \frac{1}{\zeta^n}\frac{\partial}{\partial \zeta}(\zeta^n u \tau_{\zeta\zeta}) - \frac{1}{\zeta^n}\frac{\partial}{\partial \zeta}(\zeta^n q) + Q\dot{\omega}, \tag{2.3}$$

$$\frac{\partial \rho Y}{\partial t} + \frac{1}{\zeta^n}\frac{\partial}{\partial \zeta}(\zeta^n \rho Y u) = \frac{1}{\zeta^n}\frac{\partial}{\partial \zeta}\left(\zeta^n \rho D \frac{\partial Y}{\partial \zeta}\right) - \dot{\omega}, \tag{2.4}$$

where ρ is the density, u is the velocity, p is the pressure, $\tau_{\zeta\zeta}$ and $\tau_{\phi\phi}$ are the stress tensors, q is the heat flux, e_t is the specific total internal energy, Y is the unburnt fuel mass fraction, D is the mass diffusion coefficient, $\dot{\omega}$ is the reaction rate, Q is the specific heat of reaction and t is the time. The variables n and ζ are defined as follows for the three different one-dimensional configurations considered in this paper,

$$\begin{aligned} &n = 0, \quad \zeta = x, \quad \text{planar,} \\ &n = 1, \quad \zeta = r, \quad \text{axisymmetric,} \\ &n = 2, \quad \zeta = R, \quad \text{spherically symmetric.} \end{aligned}$$

The total specific internal energy, pressure, heat flux and stress tensors may be expressed as follows:

$$e_t = \frac{1}{2}u^2 + \frac{p}{\rho(\gamma - 1)}, \tag{2.5}$$

$$p = \frac{\gamma - 1}{\gamma}\rho c_p T, \tag{2.6}$$

$$q = -k\frac{\partial T}{\partial \zeta}, \tag{2.7}$$

$$\boldsymbol{\tau}_{\zeta\zeta} = \mu\left(2\frac{\partial u}{\partial \zeta} - \frac{2}{3}\frac{1}{\zeta^n}\frac{\partial \zeta^n u}{\partial \zeta}\right), \tag{2.8}$$

and

$$\boldsymbol{\tau}_{\phi\phi} = \mu\left(2\frac{u}{\zeta} - \frac{2}{3}\frac{1}{\zeta^n}\frac{\partial \zeta^n u}{\partial \zeta}\right), \tag{2.9}$$

where T is the temperature, c_p is the specific heat capacity, k is the thermal conductivity and μ is the dynamic viscosity of the gas. By assuming a constant molecular weight mixture, the values of c_p and γ in (2.6) and (2.7) are invariant. The specific heat of reaction and the reaction rate in (2.3) and (2.4) are given by

$$Q = c_p(T_b - T_u), \tag{2.10}$$

and

$$\dot{\omega} = \Lambda \rho Y \exp\left(\frac{-\beta(1 - \Theta)}{1 - \alpha(1 - \Theta)}\right). \tag{2.11}$$

where

$$\Theta = (T - T_u)/(T_b - T_u), \tag{2.12}$$

and

$$\Lambda = B_0 \exp\left(\frac{-\beta}{\alpha}\right). \tag{2.13}$$

The variable B_0 in (2.11) is the pre-exponential factor, Θ is the reduced temperature, the subscripts u and b correspond to the unburned and burned states of the mixture, respectively. The two parameters α and β determine the flame heat release and

activation temperature, respectively (Poinsot & Veynante 2005). The following non-dimensional parameter groups define the problem:

$$Re = \left(\frac{cL}{\nu}\right)_{ref}, \tag{2.14}$$

$$Pr = \left(\frac{c_p\mu}{k}\right)_{ref}, \tag{2.15}$$

$$Sc = \left(\frac{\nu}{D}\right)_{ref}, \tag{2.16}$$

$$Le = \left(\frac{k}{\rho c_p D}\right)_{ref} = \frac{Sc}{Pr}, \tag{2.17}$$

$$Da = \left(\frac{D\Lambda}{S_L^2}\right)_{ref}, \tag{2.18}$$

$$Ma = (S_L/c)_{ref}, \tag{2.19}$$

where c is the sonic velocity, ν is the kinematic viscosity, S_L is the unstrained laminar flame speed, L is a reference length, Re is the Reynolds number, Pr is the Prandtl number, Sc is the Schmidt number, Le is the progress variable Lewis number, Da is the non-dimensional Damköhler number and Ma is the non-dimensional laminar flame speed. The subscript ref refers to the reference variables of the unburnt gas.

3. Numerical methods and flow parameters

The DNS of sound generated by a premixed flame is a challenge. Care must be taken to simultaneously ensure adequate resolution of the flame, whilst providing a large enough computational domain to resolve the larger long-wavelengths of the radiated sound. In addition, care is required at the boundaries of the computational domain to avoid spurious reflections. These requirements were achieved in the present study by using a modified form of the code NTmix. NTmix is a high-order accurate flow solver that has been used to perform DNS and LES of reactive flows using a single step chemistry. It features a sixth-order compact scheme for spatial derivatives, combined with a third-order Runge–Kutta time integrator (Cuenot, Bedet & Corjon 1997). The NTmix has been used extensively to study laminar and turbulent combustion (e.g. Poinsot & Lele 1992; Baum 1994; Bourlioux, Cuenot & Poinsot 2000), as well as non-reactive flows, such as wake vortex flows (Corjon & Poinsot 1995, 1997).

The governing equations in NTmix were modified such that the axisymmetric and spherically symmetric configurations can be simulated. The governing equations were discretised into 3000 nodes from $\zeta = 0$ to $15L_{ref}$, where L_{ref} is the reference length. Extensive grid independence studies were conducted to ensure the resolution is sufficient: there were at least 10 grid points inside the flame thickness at all times.

A symmetry boundary condition was used to simulate half of the domain in the planar case. For the axisymmetric and spherical cases, the singularity at the origin was treated using the method presented by Mohseni & Colonius (2000). The outflow boundaries were modelled with non-reflecting boundary conditions (Poinsot & Lele 1992) for the planar cases. A modified version of these boundary conditions was derived for the axisymmetic (C. S. Yoo, personal communication) and spherical cases (Talei 2011).

The flow field parameters used for different cases are presented in table 1. These parameter sets were applied to all three configurations. The Prandtl number is 0.75 for

Case	*Re*	*Da*	δ/L_{ref}	*Le*	S_L/c_{ref}	T_b/T_u	α	β
1	2000	129.616	0.1	1	0.01	4	0.75	8
2	1000	129.616	0.2	1	0.01	4	0.75	8
3	500	129.616	0.4	1	0.01	4	0.75	8

TABLE 1. Flow field parameters used for each configuration.

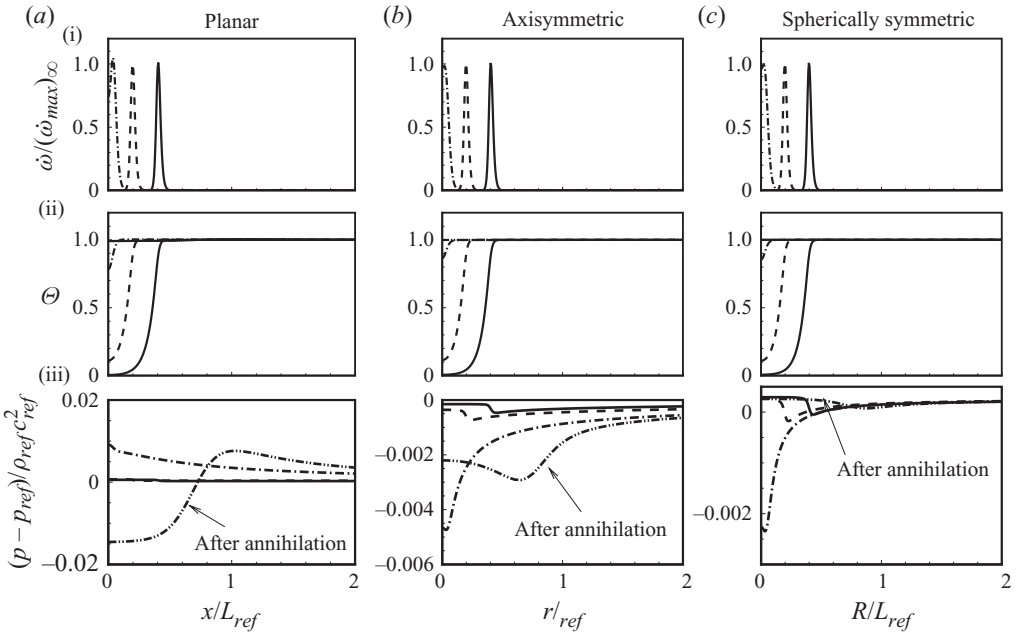

FIGURE 1. (i) Non-dimensional reaction rate $\dot{\omega}/(\dot{\omega}_{max})_\infty$, (ii) reduced temperature Θ and (iii) non-dimensional pressure $(p - p_{ref})/\rho_{ref}c_{ref}^2$ versus non-dimensional distance from the origin at different instants before (solid), during (dashed and dash-dotted) and after (dash dot dot) annihilation.

all simulations. The laminar flame thickness δ is measured using (Poinsot & Veynante 2005)

$$\delta = (T_b - T_u) \Big/ \left|\frac{\mathrm{d}T}{\mathrm{d}x}\right|_{max}. \tag{3.1}$$

The flame thickness is defined using the temperature profile when the flame is far from the origin and can be considered essentially planar.

In all simulations, the flow field is initialised with a region of unburnt gas from $\zeta = 0$ to $\zeta = 7.5L_{ref}$ that is surrounded by burnt gas from $\zeta = 7.5L_{ref}$ to $15L_{ref}$ at the adiabatic flame temperature. After initialising the flow field, the flame starts to propagate towards the origin. The propagation velocity is initially equal to the planar laminar flame speed but varies as the flame approaches the symmetry plane, axis or point (depending on the configuration).

4. Numerical results

Consider case 1 in table 1 as the baseline case. Figure 1i shows the reaction rate versus normalised distance ζ/L_{ref} at several instants. A part of the computational

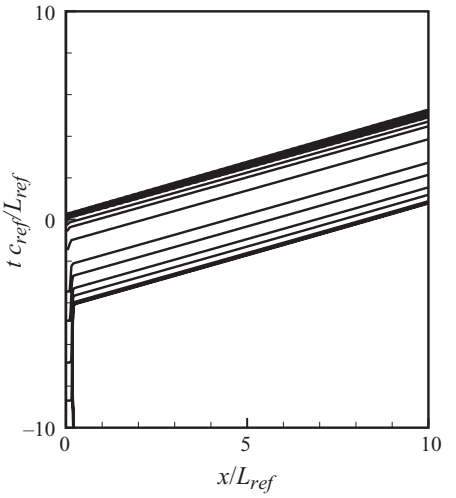

FIGURE 2. $x-t$ diagram of the pressure field during the collision of two planar flames.

domain is shown in figure 1. The flame propagates from right to left and the symmetry plane is at $\zeta/\delta = 0$. The instants are chosen as follows:

(i) 'Before' annihilation the flames are four flame thicknesses away from the origin. Negligible interaction between flames is observed.

(ii) The first instant 'during' annihilation is chosen such that the flames are two flame thicknesses away from the origin.

(iii) The second instant during annihilation is when the point of maximum heat release is close to the origin.

(iv) The instant 'after' annihilation is when the reaction has ended and the domain contains burnt gas only.

It may be observed that for each of the three configurations, the reaction rate remains close to the same spatial profile throughout. Once the flame is close to the symmetry plane, the reaction rate starts to marginally increase. Finally, as the reactants are progressively consumed, the peak reaction rate decreases until the flame is annihilated. Figure 1ii shows the reduced temperature versus normalised distance for several instants. As can be seen, the reduced temperature increases as two preheat zones start to merge for all three configurations. After the extinction event, the temperature is uniform and equal to the burnt gas temperature throughout the domain.

Now consider the pressure in the planar case, which is shown in the bottom left-most frame of figure 1. Before the annihilation event there is small, hardly observable change in the pressure profile across the flame corresponding to the pressure gradient required to accelerate the unburned gases to the positive burned gas velocity. However, during the extinction event, the pressure at the origin first increases then decreases, leading to a much larger pressure pulse that propagates away from the symmetry plane in the positive x-direction. Figures 1(b)iii and (c) show the pressure for axisymmetric and spherically symmetric cases, respectively. As the flame propagates towards the origin, the pressure difference between burnt and unburnt gas regions increase and reaches a maximum near the origin. After the annihilation event the resulting pressure wave propagates towards the outflow boundary while the pressure peak decreases.

The propagating sound wave resulting from planar flame annihilation may be observed in an $x-t$ diagram (figure 2). Here, the time $t = 0$ refers to the instant when the point of maximum reaction rate reaches the symmetry plane. At negative

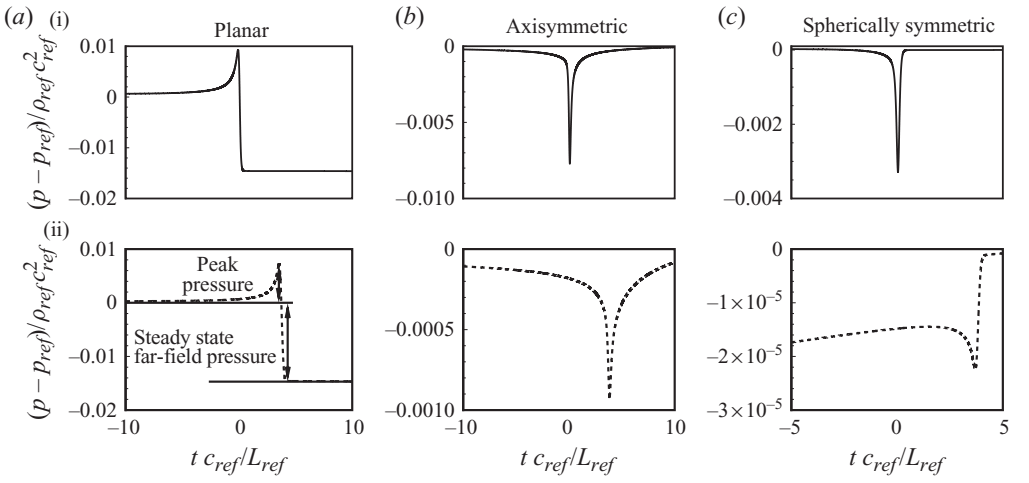

FIGURE 3. Non-dimensional pressure $(p - p_{ref})/\rho_{ref}c_{ref}^2$ for flame annihilation from simulations (i) at the symmetry axis and (ii) in the far-field $\zeta/L_{ref} = 7.5$.

times (prior to collision), the nearly vertical contour lines reflect the slow propagation of the laminar flame. During the annihilation event, acoustic energy is produced. The sound wave resulting from flame annihilation then appears as a pressure wave moving towards the outflow boundaries at the sonic velocity of the burnt gas, as evidenced by the diagonal contour lines in the $x - t$ diagram.

Figure 3 shows a comparison between a temporal history of pressure observed near the origin and in the far-field for planar, axisymmetric and spherically symmetric cases. As can be seen from figure 3i for the case of planar flame annihilation, there is a maximum in the pressure history which will be termed as the 'peak pressure'. The generated pressure wave after the annihilation event has a steady state value that is less than the reference pressure. This pressure will be referred to as the steady state far-field pressure in figure 3(*a*)ii. Note that in the planar case, the pressure in the far-field has a very similar temporal history to that at the origin.

For the axisymmetric and spherically symmetric annihilation events, a minimum is observed in the pressure history close to the origin and in the far-field. For both these cases in figure 3, the peak pressure in the far-field is small compared to the near field. This is not surprising considering the dimensionality of each problem; classical acoustics dictates a scaling of $1/\sqrt{r}$ and $1/R$ for the axisymmetric and spherically symmetric cases, respectively.

Figure 4 shows a comparison of pressure versus time at two points in the domain for each of the different configurations and different flame thicknesses. Figure 4i shows the pressure at a point near the annihilation location ($\zeta/L_{ref} = 0$ for the planar case and $\zeta/L_{ref} = 0.0025$ for the axisymmetric and spherically symmetric cases) while figure 4ii shows a point in the far-field ($\zeta/L_{ref} = 7.5$) for all three configurations and flame thicknesses. Flame thickness has negligible effect on the peak pressure near the symmetry plane in all cases. In the planar case (figure 4*a*), the steady state far-field pressure does not vary as the flame thickness is changed both at the symmetry plane and in the far-field. However, in the other two configurations, increases in the flame thickness result in significant increases in the peak pressure in the far-field.

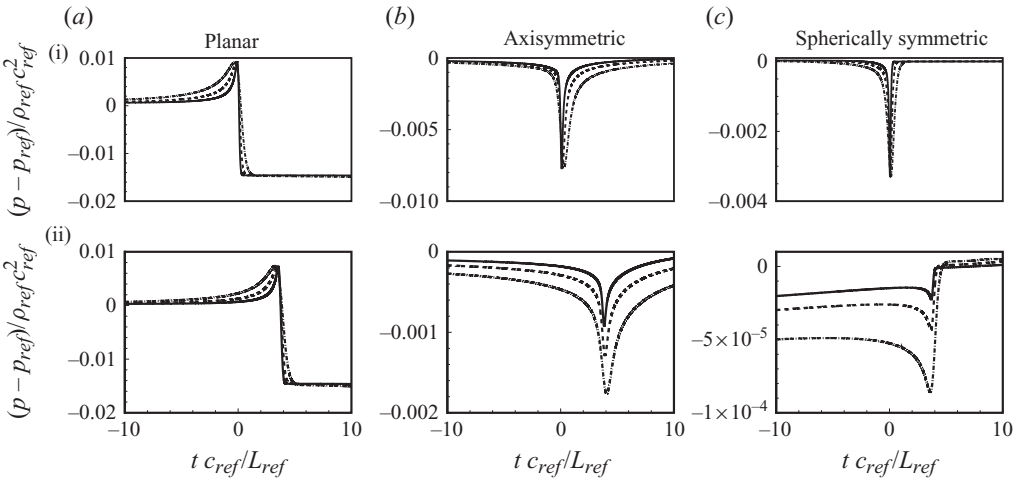

FIGURE 4. Non-dimensional pressure $(p-p_{ref})/\rho_{ref}c_{ref}^2$ for flame annihilation from simulations (i) at the symmetry axis and (ii) in the far-field $\zeta/L_{ref}=7.5$ for different flame thicknesses, $\delta/L_{ref}=0.1$ (solid line), $\delta/L_{ref}=0.2$ (dashed), $\delta/L_{ref}=0.4$ (dash-dotted).

5. Theoretical analysis

In order to investigate further the mechanism of sound generation, a theory is now developed to describe the production of sound as a function of key flame parameters. This is based on the work of Lighthill (1951). Dowling (1992) reformulated Lighthill's equation for combusting flows as follows:

$$\begin{aligned}\frac{1}{c_\infty^2}\frac{\partial^2 p}{\partial t^2}-\nabla^2 p=&\frac{\partial}{\partial t}\left(\frac{\rho_\infty}{\rho}\left(\frac{Q\dot{\omega}}{c_pT}-\frac{\boldsymbol{\nabla\cdot q}}{c_pT}+\frac{\tau_{ij}}{c_pT}\frac{\partial u_i}{\partial x_j}\right)\right)\\&+\frac{\partial^2}{\partial x_i\partial x_j}(\rho u_i u_j-\tau_{ij})\\&+\frac{1}{c_\infty^2}\frac{\partial}{\partial t}\left(\left(1-\frac{\rho_\infty c_\infty^2}{\rho c^2}\right)\frac{\mathrm{D}p}{\mathrm{D}t}-\frac{p-p_\infty}{\rho}\frac{\mathrm{D}\rho}{\mathrm{D}t}\right)\\&+\frac{\partial^2}{\partial x_i\partial t}(u_i\rho_e),\end{aligned}\tag{5.1}$$

where subscript ∞ refers to the flow field variables in the far-field. Here ρ_e is the so-called excess density,

$$\rho_e=\rho-\rho_\infty-(p-p_\infty)/c_\infty^2.\tag{5.2}$$

In a reacting flow, the first term on the right-hand side of (5.1) describes a strong monopolar source of sound (Strahle 1978; Clavin & Siggia 1991; Dowling 1992). Where combustion is unsteady and the flow Mach number is low, this term dominates the other source terms (Dowling 1992). By retaining only the source term associated with temporal fluctuations in the heat release, (5.1) can be expressed as

$$\frac{1}{c_\infty^2}\frac{\partial^2 p}{\partial t^2}-\nabla^2 p=\frac{\partial}{\partial t}\left[\frac{\rho_\infty}{\rho}\left(\frac{Q\dot{\omega}}{c_pT}\right)\right].\tag{5.3}$$

For a wave equation with $\Pi(\boldsymbol{r}, t)$ as the source term,

$$\frac{1}{c_\infty^2}\frac{\partial^2 p}{\partial t^2} - \nabla^2 p = \Pi(\boldsymbol{r}, t), \tag{5.4}$$

the solution can be obtained using a free-space Green's function (e.g. Duffy 2001),

$$p'(\boldsymbol{r}, t) = p(\boldsymbol{r}, t) - p_{ref} = \int_0^{t^+} \iiint_{V_0} G(\boldsymbol{r}, t|\boldsymbol{r_0}, \tau)\Pi(\boldsymbol{r_0}, \tau)\,\mathrm{d}V_0\,\mathrm{d}\tau, \tag{5.5}$$

where $\boldsymbol{r}$ is the position vector for any point inside or outside the source region, $\boldsymbol{r_0}$ is the position vector in the source region, V_0 is the volume of the source region and t^+ denotes the time slightly later than t and $\tau \in [0, t^+]$. The Green's functions $G(\boldsymbol{r}, t|\boldsymbol{r_0}, \tau)$ are as follows (e.g. Duffy 2001),
planar:

$$\frac{c_\infty}{2} H\left(t - \tau - \frac{|\boldsymbol{r} - \boldsymbol{r_0}|}{c_\infty}\right), \tag{5.6}$$

axisymmetric:

$$\frac{1}{2\pi}\frac{H\left(t - \tau - |\boldsymbol{r} - \boldsymbol{r_0}|/c_\infty\right)}{\sqrt{(t-\tau)^2 - |\boldsymbol{r} - \boldsymbol{r_0}|^2/c_\infty^2}}, \tag{5.7}$$

and spherically symmetric:

$$\frac{\delta(t - \tau - |\boldsymbol{r} - \boldsymbol{r_0}|/c_\infty)}{4\pi|\boldsymbol{r} - \boldsymbol{r_0}|}. \tag{5.8}$$

The heat release term in (5.3) may be re-arranged as

$$\Pi(\boldsymbol{r}, t) = \left(\frac{T_b}{T_u} - 1\right)\frac{\partial}{\partial t}\left(\frac{\rho_b T_u \dot{\omega}}{\rho T}\right), \tag{5.9}$$

where the density in the far-field is equal to the burned gas density ($\rho_\infty = \rho_b$) in this case. The term inside the second bracket on the right-hand side may be rearranged as follows:

$$\frac{\rho_b T_u \dot{\omega}}{\rho T} = \frac{\rho_b}{\rho_u}\frac{\rho_u T_u}{\rho T}\dot{\omega} = \frac{\rho_b}{\rho_u}\frac{1}{1 + p'/p_u}\dot{\omega} \tag{5.10}$$

where $p' = p - p_u$. For small p'/p_u (i.e. low Mach number flows),

$$\frac{1}{1 + p'/p_u} \approx 1. \tag{5.11}$$

With this approximation

$$\Pi(\boldsymbol{r}, t) = \left(1 - \frac{T_u}{T_b}\right)\frac{\partial}{\partial t}(\dot{\omega}(\boldsymbol{r}, t)). \tag{5.12}$$

To evaluate the theoretical assumptions up to this point, figure 5 shows a comparison of simulation results with the solution of Lighthill's equation retaining only the heat release term (5.3). The graphs show pressure at an instant after annihilation. In all cases, there is a good agreement between theory and simulation. This shows that considering the heat release term as the main mechanism of sound generation is a reasonable assumption.

Given the rate of reaction, (5.5) and (5.12) provide a means of determining sound production. In the ensuing sections, particular results for each configuration are now developed under increasingly restrictive assumptions.

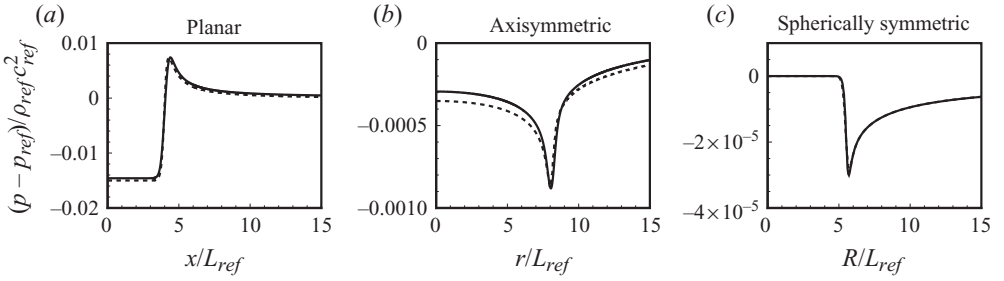

FIGURE 5. Non-dimensional pressure $(p - p_{ref})/\rho_{ref}c_{ref}^2$ for the planar, axisymmetric and spherically symmetric flame annihilation from simulations (solid line), solution of (5.3) (dashed), $\delta/L_{ref} = 0.1$.

5.1. *Flames of finite thickness*

Recall that figure 1 showed that the spatial variation of reaction rate relative to the moving flame location, was fairly time invariant. Therefore, the reaction rate may be modelled as a temporally invariant function of space relative to a moving flame location $\zeta_f(\tau)$, i.e.

$$\dot{\omega}(\zeta, \tau) = f(\zeta_f(\tau) - |\zeta|), \tag{5.13}$$

where $\zeta_f(\tau)$ represents the instantaneous flame location, and defined in this study as the location of the maximum reaction rate. The variable ζ is the axial coordinate in the planar configuration and the radial coordinate in the axisymmetric and spherically symmetric configurations. Furthermore, when the flame is far from the origin, the integral of the function may be easily shown to be

$$\int_0^{+\infty} f(\zeta_f - |\zeta|)\,\mathrm{d}\zeta = \rho_u S_L. \tag{5.14}$$

In the ensuing sections, both (5.13) and (5.14) will be invoked in their expected region of validity – when the flame is reasonably far from the origin, specifically when $\zeta_f >> \delta_L$.

5.1.1. *Planar flame annihilation*

Using the Green's function solution of (5.3), the pressure may be obtained in the far-field,

$$\begin{aligned} p'(x,t) &= \frac{c_b}{2}\left(1-\frac{T_u}{T_b}\right)\int_{-\zeta^+}^{+\zeta^+}\int_0^{t-\frac{|x-\zeta|}{c_b}} \frac{\partial\dot{\omega}}{\partial\tau}\,\mathrm{d}\zeta\,\mathrm{d}\tau, \\ &= \frac{c_b}{2}\left(1-\frac{T_u}{T_b}\right)\int_{-\zeta^+}^{+\zeta^+} \dot{\omega}\left(\zeta, t-\frac{|x-\zeta|}{c_b}\right)\mathrm{d}\zeta - \frac{c_b}{2}\left(1-\frac{T_u}{T_b}\right)\int_{-\zeta^+}^{+\zeta^+}\dot{\omega}(\zeta,0)\,\mathrm{d}\zeta, \end{aligned} \tag{5.15}$$

where ζ^+ specifies the size of the source region. The second integral term on the right-hand side of (5.15) is proportional to the integral of the reaction rate of the two flames before the collision event and can be obtained using (5.14),

$$\frac{c_b}{2}\left(1-\frac{T_u}{T_b}\right)\int_{-\zeta^+}^{+\zeta^+}\dot{\omega}(\zeta,0)\,\mathrm{d}\zeta = \rho_u c_b\left(1-\frac{T_u}{T_b}\right)S_L. \tag{5.16}$$

The first integral term on the right-hand side of (5.15) can be evaluated by assuming that $|x| \longrightarrow \infty$ and so $|x-\zeta| \approx |x|$. If τ_1 is defined as the instant that the total integrated reaction rate starts to change when the flame is close to the origin (recall figure 1) and τ_2 as the instant at which the flame has just disappeared, the first integral term in (5.15) can be obtained,

$$\int_{-\zeta^+}^{+\zeta^+} \dot{\omega}\left(\zeta, t-\frac{|x-\zeta|}{c_b}\right) \mathrm{d}\zeta = \begin{cases} 2\rho_u S_L, & t-|x|/c_b < \tau_1, \\ \dot{\omega}_T(t-|x|/c_b), & \tau_1 < t-|x|/c_b < \tau_2, \\ 0, & \tau_2 < t-|x|/c_b, \end{cases} \tag{5.17}$$

where $\dot{\omega}_T$ is the instantaneous total reaction rate (i.e. the reaction rate integrated over space). Considering (5.16) and (5.17), the general solution for the pressure in the planar case can, therefore, be described as

$$p'(x,t) = \begin{cases} 0, & t-|x|/c_b < \tau_1, \\ \rho_u c_b\left(1-\dfrac{T_u}{T_b}\right) S_L\left(\dfrac{\dot{\omega}_T(t-|x|/c_b)}{\rho_u S_L}-1\right), & \tau_1 < t-|x|/c_b < \tau_2, \\ -\rho_u c_b\left(1-\dfrac{T_u}{T_b}\right) S_L, & \tau_2 < t-|x|/c_b. \end{cases} \tag{5.18}$$

Equation (5.18) has three parts. The first part of the solution ($t-|x|/c_b < \tau_1$) shows that the net sound production where the flame is reasonably far from the symmetry plane is zero, as expected. The second part ($\tau_1 < t-|x|/c_b < \tau_2$) corresponds to when the annihilation event occurs and the total reaction rate starts to change. In the last term ($\tau_2 < t-|x|/c_b$), the sound produced as a result of complete annihilation appears as a constant negative pressure wave. This instant is when the acoustic wave produced during collision has passed the observer located at x, resulting in the steady state far-field pressure,

$$p'(x,t) = -\rho_u c_b\left(1-\frac{T_u}{T_b}\right) S_L. \tag{5.19}$$

The theory therefore suggests that the steady state pressure change is independent of flame thickness and linearly dependent on flame speed.

5.1.2. *Axisymmetric flame annihilation*

Again considering only the far-field, $|\boldsymbol{r}| \longrightarrow \infty$ and so $|\boldsymbol{r}-\boldsymbol{r_0}| \approx |\boldsymbol{r}|$, the pressure can be expressed as

$$p'(r,t) = \left(1-\frac{T_u}{T_b}\right) \int_0^{t-r/c_b} \int_0^{\zeta^+} \frac{\zeta\, \partial\dot{\omega}/\partial\tau}{\sqrt{(t-\tau)^2 - r^2/c_b^2}} \mathrm{d}\zeta\, \mathrm{d}\tau. \tag{5.20}$$

Equation (5.20) shows that analysis of this axisymmetric flame is slightly more difficult than that of the planar case because of the time-dependent Green's function. In order to evaluate this integral, the following cases are considered.

Case 1: $t-r/c_b < \tau_1$

Where the flame is moving towards the origin and before there is significant flame curvature, the integral can be obtained using the following:

$$\int_0^{\zeta^+} \zeta \frac{\partial\dot{\omega}}{\partial\tau}\, \mathrm{d}\zeta = -S_L \int_0^{\zeta^+} \zeta f'(\zeta_f - \zeta)\, \mathrm{d}\zeta. \tag{5.21}$$

This integral can be calculated using integration by parts

$$\int_0^{\zeta^+} \zeta f'(\zeta_f - \zeta)\,\mathrm{d}\zeta = \zeta f(\zeta_f - \zeta)\Big|_0^{\zeta^+} - \int_0^{\zeta^+} f(\zeta_f - \zeta)\,\mathrm{d}\zeta. \tag{5.22}$$

Since the boundary of the source region is always chosen to be outside the flame, the first term on the right-hand side in (5.22) is zero. Therefore, the solution can be obtained as a function of the total integrated reaction rate,

$$p'(r,t) = -\left(1 - \frac{T_u}{T_b}\right) S_L \int_0^{t-r/c_b} \frac{\displaystyle\int_0^{\zeta^+} f(\zeta_f - \zeta)\,\mathrm{d}\zeta}{\sqrt{(t-\tau)^2 - r^2/c_b^2}}\,\mathrm{d}\tau. \tag{5.23}$$

Since at any $t < \tau_1$ the propagation velocity is approximately constant, (5.23) may be evaluated as

$$\begin{aligned} p'(r,t) &= -\rho_u S_L^2 \left(1 - \frac{T_u}{T_b}\right) \int_0^{t-r/c_b} \frac{\mathrm{d}\tau}{\sqrt{(t-\tau)^2 - r^2/c_b^2}} \\ &= -\rho_u S_L^2 \left(1 - \frac{T_u}{T_b}\right) H(t - r/c_b) \ln\left(\frac{r/c_b}{t - \sqrt{t^2 - r^2/c_b^2}}\right). \end{aligned} \tag{5.24}$$

Case 2: $t - r/c_b > \tau_1$

In this case the solution can be obtained by dividing the time period of the integral into two parts: $(0, \tau_1)$ and $(\tau_1, t - r/c_b)$, i.e.,

$$\begin{aligned} p'(r,t) &= -\rho_u S_L^2 \left(1 - \frac{T_u}{T_b}\right) \int_0^{\tau_1} \frac{\mathrm{d}\tau}{\sqrt{(t-\tau)^2 - r^2/c_b^2}} \\ &\quad + \left(1 - \frac{T_u}{T_b}\right) \int_{\tau_1}^{t-r/c_b} \int_0^{\zeta^+} \frac{\zeta\,\partial\dot{\omega}/\partial\tau}{\sqrt{(t-\tau)^2 - r^2/c_b^2}}\,\mathrm{d}\zeta\,\mathrm{d}\tau, \\ &= -\rho_u S_L^2 \left(1 - \frac{T_u}{T_b}\right) H(t - r/c_b) \ln\left(\frac{r/c_b}{t - \tau_1 - \sqrt{(t-\tau_1)^2 - r^2/c_b^2}}\right) \\ &\quad + \left(1 - \frac{T_u}{T_b}\right) \int_{\tau_1}^{t-r/c_b} \int_0^{\zeta^+} \frac{\zeta\,\partial\dot{\omega}/\partial\tau}{\sqrt{(t-\tau)^2 - r^2/c_b^2}}\,\mathrm{d}\zeta\,\mathrm{d}\tau. \end{aligned} \tag{5.25}$$

General solution

The general solution can be expressed using the Heaviside function by combining cases 1 and 2,

$$\begin{aligned} p'(r,t) &= -\rho_u \left(1 - \frac{T_u}{T_b}\right) S_L^2 H(t - r/c_b) \left\{ \ln\left(\frac{r/c_b}{t - \sqrt{t^2 - r^2/c_b^2}}\right) \right. \\ &\quad \left. + H\left[c_b(t - \tau_1) - r\right] \ln\left(\frac{t - \tau_1 - \sqrt{(t-\tau_1)^2 - r^2/c_b^2}}{r/c_b}\right) \right\} \\ &\quad + \left(1 - \frac{T_u}{T_b}\right) \int_{\tau_1}^{t-r/c_b} \int_0^{\zeta^+} \frac{\zeta\,\partial\dot{\omega}/\partial\tau}{\sqrt{(t-\tau)^2 - r^2/c_b^2}}\,\mathrm{d}\zeta\,\mathrm{d}\tau. \end{aligned} \tag{5.26}$$

This result is quite general as the assumption that the flame is propagating at constant speed with a time-invariant profile prior to the time τ_1 is expected to be valid as long as τ_1 is chosen such that the flame is sufficiently far from the origin.

5.1.3. *Spherically symmetric flame annihilation*

Again considering only the far-field, the solution of the wave equation uses a similar argument as for the axisymmetric case (§ 5.1.2),

$$p'(r,t) = \left(1 - \frac{T_u}{T_b}\right) H(t - R/c_b) \frac{\displaystyle\int_0^{\zeta^+} \zeta^2 \partial\dot{\omega}/\partial\tau \, \mathrm{d}\zeta|_{\tau=t-R/c_b}}{R}. \tag{5.27}$$

For $\tau < \tau_1$, the integral term may be obtained using (5.13),

$$\int_0^{\zeta^+} \zeta^2 \frac{\partial\dot{\omega}}{\partial\tau} \, \mathrm{d}\zeta = -S_L \int_0^{\zeta^+} \zeta^2 f'(\zeta_f - \zeta) \, \mathrm{d}\zeta. \tag{5.28}$$

Using an analogous approach to the axisymmetric case,

$$p'(r,t) = -2\left(1 - \frac{T_u}{T_b}\right) S_L H(t - R/c_b) \frac{\displaystyle\int_0^{\zeta^+} \zeta f(\zeta_f - \zeta) \, \mathrm{d}\zeta|_{\tau=t-R/c_b}}{R}. \tag{5.29}$$

Unlike the axisymmetric case the integral in (5.29) is not independent of the reaction rate profile. If the flame is thin, the integral will be dominated by the values close to ζ_f, and

$$\int_0^{\zeta^+} \zeta f(\zeta_f - \zeta) \, \mathrm{d}\zeta \sim \zeta_f \int_0^{\zeta^+} f(\zeta_f - \zeta) \, \mathrm{d}\zeta = \zeta_f \rho_u S_L. \tag{5.30}$$

Now, the solution for $t - R/c_b < \tau_1$ may be obtained,

$$p'(r,t) = -2\rho_u \left(1 - \frac{T_u}{T_b}\right) S_L^2 \zeta_f (t - R/c_b) H(t - R/c_b)/R. \tag{5.31}$$

Using (5.31), the general solution may be expressed as

$$\begin{aligned} p'(r,t) = {} & -2\rho_u \left(1 - \frac{T_u}{T_b}\right) S_L^2 H(t - R/c_b) \zeta_f (t - R/c_b) H[\tau_1 - (t - R/c_b)] \\ & + \left(1 - \frac{T_u}{T_b}\right) H(t - R/c_b) \{1 - H[\tau_1 - (t - R/c_b)]\} \frac{\displaystyle\int_0^{\zeta^+} \zeta^2 \partial\dot{\omega}/\partial\tau \, \mathrm{d}\zeta|_{\tau=t-R/c_b}}{R}. \end{aligned} \tag{5.32}$$

Comparison of (5.32) and (5.26) shows that when the flame is sufficiently far from the origin (i.e. $t - r/c_b < \tau_1$ for axisymmetric and $t - R/c_b < \tau_1$ for spherically symmetric case) the pressure fluctuations is proportional to $\rho_u (1 - (T_u/T_b)) S_L{}^2$ for both axisymmetric and spherically symmetric cases.

5.2. *Flames of zero thickness*

The special case of an infinitely thin flame is now developed. For a flame of zero thickness, the flow field variables can be modelled using a Heaviside function,

$$\rho = (\rho_u - \rho_b) H(\zeta_f - |\zeta|) + \rho_b, \quad Y = H(\zeta_f - |\zeta|). \tag{5.33}$$

Substituting these functions into (2.4) and assuming $\zeta > 0$,

$$-\rho_u V_f \delta(\zeta_f - \zeta) = -\frac{n}{\zeta}\rho_u D\delta(\zeta_f - \zeta) + \rho_u D\delta'(\zeta_f - \zeta) - \dot{\omega}, \tag{5.34}$$

where V_f is the flame propagation velocity

$$V_f(\tau) = -\frac{\mathrm{d}\zeta_f}{\mathrm{d}\tau}. \tag{5.35}$$

It may be noted that we can replace ζ with ζ_f in the first term on the right-hand side of (5.34) since for other values of ζ this term will be equal to zero. In order to obtain the solutions for each configuration, (5.34) is multiplied by ζ^n and integrated across the flame,

$$\int_0^{\zeta^+} \zeta^n \dot{\omega}\, \mathrm{d}\zeta = \rho_u \zeta_f^n V_f(\tau) H(\zeta_f). \tag{5.36}$$

Therefore, the spatial integral can be obtained as follows:

$$\int_0^{\zeta^+} \zeta^n \frac{\partial \dot{\omega}}{\partial \tau}\, \mathrm{d}\zeta = \rho_u \left(\zeta_f^n \frac{\partial V_f}{\partial \tau} - n\zeta_f^{n-1} V_f^2\right) H(\zeta_f). \tag{5.37}$$

5.2.1. *Planar flame annihilation*

For a flame of zero thickness, the first integral term in (5.15) can be expressed in the form of a Heaviside function

$$\int_{-\zeta^+}^{+\zeta^+} \dot{\omega}\left(\zeta, t - \frac{|x-\zeta|}{c_b}\right) \mathrm{d}\zeta = \rho_u V_f(\tau) H(\zeta_f(\tau))|_{\tau = t - |x|/c_b}, \tag{5.38}$$

and, therefore, the solution for a flame of zero thickness may be obtained,

$$p'(x,t) = \rho_u c_b \left(1 - \frac{T_u}{T_b}\right) S_L H(t - |x|/c_b) \left(\frac{V_f(\tau)}{S_L} H(\zeta_f(\tau)) - 1\right)|_{\tau = t - |x|/c_b}. \tag{5.39}$$

Equation (5.39) shows that the steady state far-field pressure (i.e. as $t \longrightarrow \infty$) is the same as that obtained from the theoretical analysis for finite flame thickness analysis. Also since peak pressure will occur where the flame collides with the symmetric plane, the peak pressure may be obtained,

$$p_{peak} = \rho_u c_b \left(1 - \frac{T_u}{T_b}\right)\left(V_f(\tau_e) - S_L\right), \tag{5.40}$$

where τ_e refers to the extinction instant (i.e. $\zeta_f(\tau_e) = 0$). Equation (5.40) shows that in order to calculate the peak pressure, the propagation velocity at the collision instant needs to be estimated.

5.2.2. *Axisymmetric flame annihilation*

Equation (5.37) is used to evaluate the integral in (5.20). For $n = 1$ in (5.37),

$$\int_0^{\zeta^+} \zeta \frac{\partial \dot{\omega}}{\partial \tau}\, \mathrm{d}\zeta = \rho_u \left(-V_f^2 + \frac{\partial V_f}{\partial \tau}\zeta_f\right) H(\zeta_f). \tag{5.41}$$

Therefore, the solution may be obtained,

$$p'(r,t) = \rho_u \left(1 - \frac{T_u}{T_b}\right) \int_0^{t - r/c_b} \frac{(-V_f(\tau)^2 + \zeta_f \partial V_f/\partial \tau) H(\zeta_f)}{\sqrt{(t-\tau)^2 - r^2/c_b^2}}\, \mathrm{d}\tau. \tag{5.42}$$

Equation (5.42) shows the pressure fluctuation in the far-field depends on both the propagation velocity and time derivative of propagation velocity. However, at the extinction instant it is only a function of propagation velocity. This dependency is similar to the planar flame annihilation results for the peak pressure.

5.2.3. *Spherically symmetric flame annihilation*

For a flame of zero thickness and using (5.37),

$$p'(R,t) = \rho_u \left(1 - \frac{T_u}{T_b}\right) \left(-2\zeta_f V_f^2 + \zeta_f^2 \frac{\partial V_f}{\partial \tau}\right) H(\tau) H(\zeta_f(\tau))/R|_{\tau=t-R/c_b}, \tag{5.43}$$

which is the result obtained by Thomas & Williams (1966) for inward burning thin flames.

5.3. *Flames of zero thickness propagating at S_L*

5.3.1. *Planar flame annihilation*

Assuming a constant propagation velocity $V_f = S_L$, the flame position can be described as

$$\zeta_f = \zeta_0 - S_L \tau, \tag{5.44}$$

where ζ_0 is the initial position of the flame. Therefore, the solution of the wave equation can be obtained from (5.39),

$$p'(x,t) = -\rho_u c_b \left(1 - \frac{T_u}{T_b}\right) S_L H(t - |x|/c_b) H\left[S_L\left(t - \frac{|x|}{c_b}\right) - \zeta_0\right]. \tag{5.45}$$

Equation (5.45) features a Heaviside function $H(x,t)$ travelling at the speed of sound in the burned gas. The steady state far-field pressure in (5.45) can be rearranged in a non-dimensional form as a function of temperature ratio and laminar flame speed,

$$\frac{p'}{\rho_u c_u^2} = -\frac{S_L}{c_u}\left(1 - \frac{T_u}{T_b}\right)\sqrt{\frac{T_b}{T_u}}. \tag{5.46}$$

5.3.2. *Axisymmetric flame annihilation*

Assuming constant propagation velocity ($V_f = S_L$ and $\partial V_f/\partial \tau = 0$), the solution can be obtained from (5.42),

$$\begin{aligned} p'(r,t) &= -\rho_u {S_L}^2 \left(1 - \frac{T_u}{T_b}\right) \int_0^{t-r/c_b} \frac{\mathrm{d}\tau}{\sqrt{(t-\tau)^2 - r^2/c_b^2}} \\ &= -\rho_u \left(1 - \frac{T_u}{T_b}\right) {S_L}^2 H(t - r/c_b) \left\{ \ln\left(\frac{r/c_b}{t - \sqrt{t^2 - r^2/c_b^2}}\right) \right. \\ &\quad \left. + H\left[c_b(t-\tau_1) - r\right] \ln\left(\frac{t - \tau_1 - \sqrt{(t-\tau_1)^2 - r^2/c_b^2}}{r/c_b}\right)\right\}. \end{aligned} \tag{5.47}$$

Comparison of (5.47) and (5.26) shows that the general finite thickness solution in (5.26) includes the solution for a flame of zero thickness and constant flame speed plus a contribution of sound produced during the annihilation. This second term is dependent on the dynamics of the annihilation event. Equation (5.26) shows that for a flame of zero thickness with a constant propagation velocity and reaction rate profile the integral term will be zero because τ_1 is the extinction instant and at any instant after τ_1 we have a source free region.

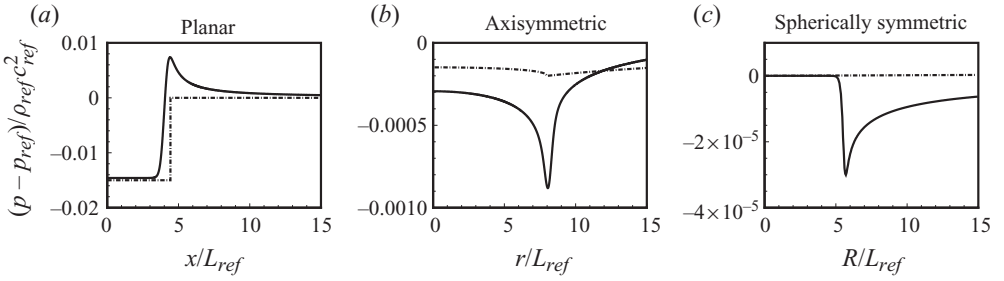

FIGURE 6. Non-dimensional pressure $(p - p_{ref})/\rho_{ref}c_{ref}^2$ for the planar, axisymmetric and spherically symmetric flame annihilation from simulations (solid line), zero flame thickness (dash-dotted).

5.3.3. *Spherically symmetric flame annihilation*

The pressure in the far-field for a constant propagation velocity ($V_f = S_L$) may be determined from (5.43),

$$p'(r,t) = -2\rho_u {S_L}^2 \left(1 - \frac{T_u}{T_b}\right)(\zeta_0 - S_L(t - R/c_b))H(\zeta_0 - S_L(t - R/c_b))H(t - R/c_b)/R. \tag{5.48}$$

Similar to the axisymmetric case, (5.48) is a part of the general finite thickness solution (5.32).

5.4. *Discussion of the theoretical results*

The simulation results for axisymmetric and spherically symmetric flame annihilation both demonstrated that the flame thickness had a significant effect on the far-field sound produced (figure 4). The corresponding theoretical results for the far-field sound ((5.26) and (5.27)) both featured terms which require integration over the flame thickness, and so potentially incorporate this observed effect into a theory of sound production.

Figure 6 compares the zero flame thickness results with simulation ((5.45), (5.47) and (5.48)). The graphs show the pressure versus x, r and R at some instant after annihilation. In the case of planar flame annihilation, the predicted step change in the pressure agrees with the numerical results. In the case of axisymmetric and spherically symmetric flame annihilations, it is clear that the zero flame thickness result significantly underestimates the sound production. Thus, comparison of figures 5 and 6 is direct evidence that the source term in (5.3) is the dominant source term in the problem, and that the flame thickness and the dynamics of the annihilation event need to be taken into account.

Considering now in more detail the dynamics of the annihilation event, figure 7(*a*) shows the total integrated reaction rate versus flame position for case 1 in table 1. (The point of maximum reaction rate is defined as the flame position in this study.) The total reaction rate is similar for all three configurations and is not constant during the annihilation event. Indeed, the total integrated reaction rate starts to change when the flame is roughly two flame thicknesses away from the origin for all configurations. Similarly, figure 7(*b*) shows that the flame starts to accelerate prior to annihilation. Significant variations in the propagation velocity V_f during flame annihilation have also been observed by others (see, for example, Chen & Sohrab 1995; Echekki *et al.*

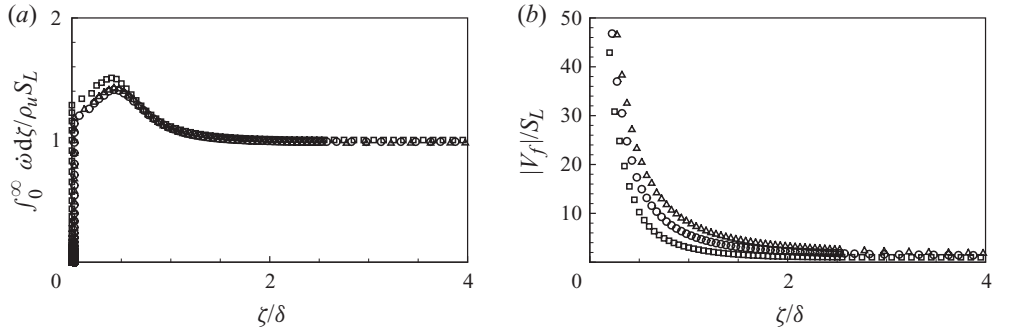

FIGURE 7. (*a*) Normalised total reaction rate: $\int_0^\infty \dot{\omega}\mathrm{d}\zeta/\rho_u S_L$, (*b*) magnitude of normalised propagation velocity: $|V_f|/S_L$ versus ζ/δ, square: planar case, circle: axisymmetric case, delta: spherically symmetric case.

1996; Wichman & Vance 1997; Petrov & Ghoniem 1998; Sun & Law 1998; Lu & Ghosal 2003).

Returning to the acoustic theory in § 5.2, V_f was identified as a key parameter in expanded forms of the source term in (5.3), and so is a key parameter in the sound production. The relative contribution of reaction rate, diffusion and curvature effects have been observed to drive these variations, such that V_f can be obtained using the following equation (Gibson 1968; Echekki & Chen 1999):

$$\boldsymbol{V_f} = \boldsymbol{u} + S_d \boldsymbol{n_f}, \tag{5.49}$$

where $\boldsymbol{n_f} = \nabla Y/|\nabla Y|$ and S_d is the displacement velocity,

$$S_d = -\frac{\dot{\omega}}{\rho|\nabla Y|} - \frac{\nabla\cdot(\rho D \nabla Y)}{\rho|\nabla Y|}. \tag{5.50}$$

Equations (5.49) and (5.50) can be rearranged such that the effect of curvature can be observed,

$$\boldsymbol{V_f} = \boldsymbol{u} - \underbrace{\frac{\dot{\omega}}{\rho|\nabla Y|}\boldsymbol{n_f}}_{\text{Term I}} - \underbrace{\frac{\dfrac{\partial}{\partial\zeta}\left(\rho D \dfrac{\partial Y}{\partial\zeta}\right)}{\rho|\nabla Y|}\boldsymbol{n_f}}_{\text{Term II}} - \underbrace{D(\nabla\cdot\boldsymbol{n_f})\boldsymbol{n_f}}_{\text{Term III}}. \tag{5.51}$$

Figure 8 shows the contribution of each term in (5.51) to the increase in the propagation velocity for all configurations. As can be seen, the curvature term in (5.51) accounts for the differences in V_f for the planar, axisymmetric and spherically symmetric cases. This demonstrates that flame acceleration should start at a progressively greater distance from the origin in the axisymmetric and spherically symmetric cases, as observed in figure 7(*b*), and that the results of this study are consistent with those reported in other studies concerned with the dynamics of premixed flame annihilation.

Thus, the results in figures 6, 7 and 8 are consistent. By not including the increased reaction rate and significant flame acceleration observed in figure 7, the sound produced by the zero flame thickness results in figure 6 should underestimate the simulation result.

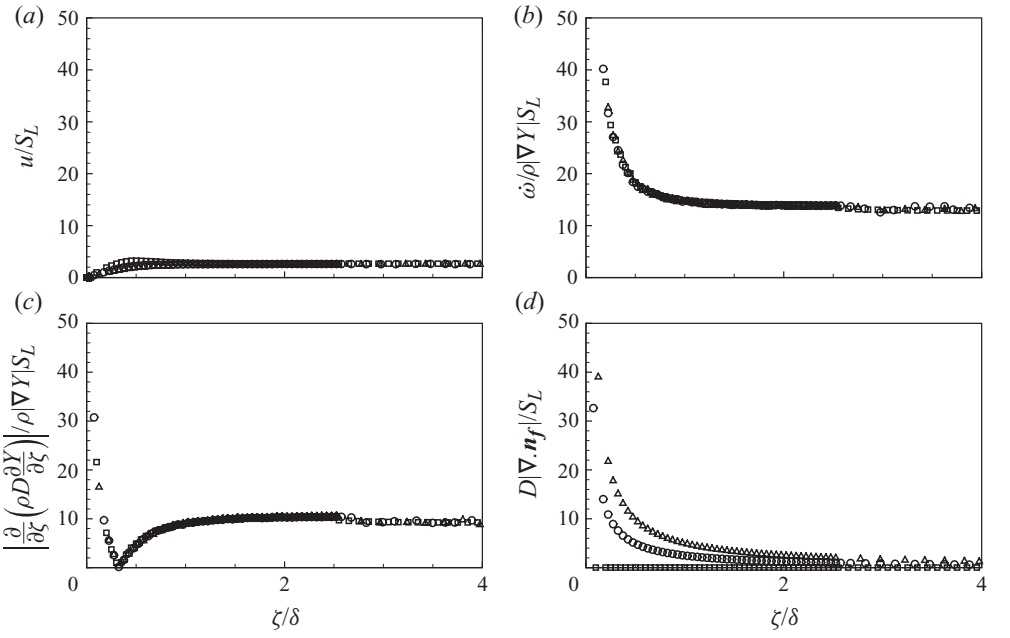

FIGURE 8. (*a*) Normalised gas velocity: u/S_L, magnitude of (*b*) term I, (*c*) term II and (*d*) term III in (5.51) normalised by S_L versus ζ/δ, square: planar case, circle: axisymmetric case, delta: spherically symmetric case.

5.5. *Non-dimensionalising the theoretical solutions*

Figure 9 shows the effect of flame thickness for three different flames thicknesses listed in table 1. As can be seen there is almost no difference between all three cases when plotted as a function of ζ/δ, demonstrating that the annihilation events scale with the flame thickness in all cases. This is not surprising since the flame thickness is the only length scale in the problem other than the initial flame position, which has a very small effect on the results.

The propagation velocity is also equal to the laminar flame speed in the far-field. The following reference parameters are, therefore, chosen:

$$\bar{\zeta} = \frac{\zeta}{\delta}, \quad \bar{t} = \frac{tS_L}{\delta}. \tag{5.52}$$

Using these non-dimensional parameters, the general solutions for the finite thickness flames are

$$\frac{p'}{\rho_u c_u^2} = \frac{S_L}{c_u}\left(1 - \frac{T_u}{T_b}\right)\sqrt{\frac{T_b}{T_u}}\left(\int_0^{\bar{\zeta}^+} \bar{\omega}(\bar{\zeta}, \bar{t} - \bar{x}/\bar{c_b})\,\mathrm{d}\bar{\zeta} - 1\right), \tag{5.53}$$

for the planar case,

$$\frac{p'}{\rho_u c_u^2} = \left(\frac{S_L}{c_u}\right)^2\left(1 - \frac{T_u}{T_b}\right)\int_0^{\bar{t}-\bar{r}/\bar{c_b}}\int_0^{\bar{\zeta}^+} \frac{\bar{\zeta}\,\partial\bar{\omega}/\partial\bar{\tau}}{\sqrt{(\bar{t}-\bar{\tau})^2 - \bar{r}^2/\bar{c_b}^2}}\,\mathrm{d}\bar{\zeta}\,\mathrm{d}\bar{\tau}, \tag{5.54}$$

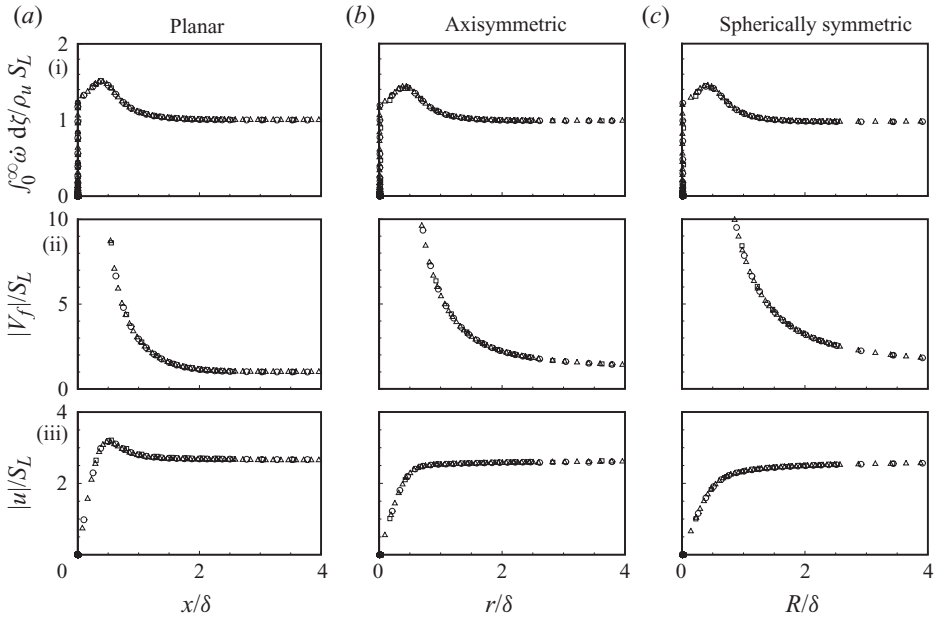

FIGURE 9. (i) Normalised total reaction rate: $\int_0^\infty \dot{\omega}\,\mathrm{d}\zeta/\rho_u S_L$, (ii) magnitude of normalised propagation velocity: $|V_f|/S_L$, (iii) normalised gas velocity: $|u|/S_L$ versus ζ/δ, square: $\delta = 0.1$, circle: $\delta = 0.2$, delta: $\delta = 0.4$.

for the axisymmetric case and,

$$\frac{p'}{\rho_u c_u^2} = \left(\frac{S_L}{c_u}\right)^2 \left(1 - \frac{T_u}{T_b}\right) \frac{\displaystyle\int_0^{\bar{\zeta}^+} \bar{\zeta}^2 \partial\bar{\omega}/\partial\bar{\tau}\,\mathrm{d}\bar{\zeta}|_{\bar{\tau}=\bar{t}-\bar{R}/\bar{c}_b}}{\bar{R}}, \tag{5.55}$$

for the spherically symmetric case.

Equation (5.53) shows that the pressure history in the far-field of the planar annihilation event is not a function of flame thickness, which is consistent with the simulation results. In order to analyse the axisymmetric results, some further simplification is required. The term in the denominator of (5.54) can be factorised,

$$(\bar{t} - \bar{\tau})^2 - \bar{r}^2/\bar{c_b}^2 = [(\bar{t} - \bar{\tau}) - \bar{r}/\bar{c_b}]\,[(\bar{t} - \bar{\tau}) + \bar{r}/\bar{c_b}]\,. \tag{5.56}$$

Equation (5.56) becomes singular when $(\bar{t} - \bar{\tau}) = \bar{r}/\bar{c_b}$, which is one terminal of the definite integral in $\bar{\tau}$ in (5.54). As Dowling & Ffowcs Williams (1983) therefore argue, the first term dominates the second term on the right-hand side of (5.56), leading to the approximation

$$(\bar{t} - \bar{\tau})^2 - \bar{r}^2/\bar{c_b}^2 = 2\bar{r}/\bar{c_b}\,[(\bar{t} - \bar{\tau}) - \bar{r}/\bar{c_b}]\,. \tag{5.57}$$

This implies that

$$\frac{p'}{\rho_u c_u^2} \propto \sqrt{\frac{\bar{c_b}}{\bar{r}}} = \sqrt{\frac{c_b}{S_L}}\sqrt{\frac{\delta}{r}} = \left(\frac{T_b}{T_u}\right)^{1/4} \left(\frac{S_L}{c_u}\right)^{-(1/2)} \left(\frac{\delta}{r}\right)^{1/2}. \tag{5.58}$$

In the case of spherically symmetric annihilation, it may be observed from (5.55) that

$$\frac{p'}{\rho_u c_u^2} \propto \frac{1}{\bar{R}} = \frac{\delta}{R}. \tag{5.59}$$

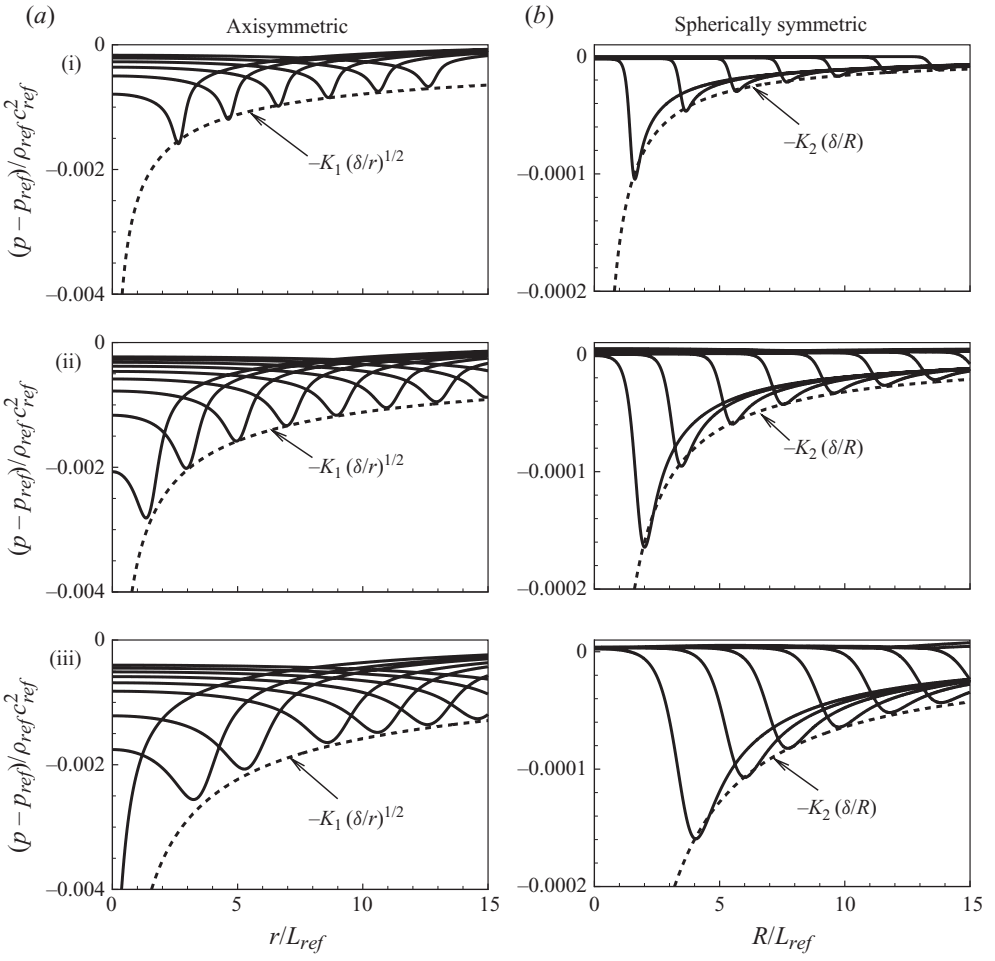

FIGURE 10. Non-dimensional pressure $(p - p_{ref})/\rho_{ref}c_{ref}^2$ versus radius after the annihilation event for several time instants and different flame thicknesses: (i) $\delta/L_{ref} = 0.1$, (ii) $\delta/L_{ref} = 0.2$ and (iii) $\delta/L_{ref} = 0.4$.

Figure 10 shows pressure versus radius in the axisymmetric and spherically symmetric flame annihilations for several instants after extinction and different flame thicknesses. As can be seen the curves joining the pressure peaks follow (5.58) and (5.59) closely. The variables K_1 and K_2 are equal to 0.0079 and 0.0016, respectively. This confirms the importance of flame thickness on sound production.

Combining these results, the scaling of the problem can now be stated. For planar annihilation,

$$\frac{p'}{\rho_u c_u^2} \sim \left(\frac{S_L}{c_u}\right)\left(\frac{\delta}{x}\right)^0 \left(1-\frac{T_u}{T_b}\right)\left(\frac{T_b}{T_u}\right)^{(1/2)} g_1\left(\frac{T_b}{T_u}, x, t\right), \tag{5.60}$$

for axisymmetric annihilation,

$$\frac{p'}{\rho_u c_u^2} \sim \left(\frac{S_L}{c_u}\right)^{3/2}\left(\frac{\delta}{r}\right)^{1/2} \left(1-\frac{T_u}{T_b}\right)\left(\frac{T_b}{T_u}\right)^{(1/4)} g_2\left(\frac{T_b}{T_u}, r, t\right), \tag{5.61}$$

and for spherically symmetric annihilation,

$$\frac{p'}{\rho_u c_u^2} \sim \left(\frac{S_L}{c_u}\right)^2 \left(\frac{\delta}{R}\right)^1 \left(1 - \frac{T_u}{T_b}\right) g_3\left(\frac{T_b}{T_u}, R, t\right). \tag{5.62}$$

More generally these can be written as

$$\frac{p'}{\rho_u c_u^2} \sim \left(\frac{S_L}{c_u}\right)^{1+(n/2)} \left(\frac{\delta}{\zeta}\right)^{n/2} \left(1 - \frac{T_u}{T_b}\right) \left(\frac{T_b}{T_u}\right)^{(2-n)/4} g\left(\frac{T_b}{T_u}, \zeta, t\right), \tag{5.63}$$

where function g describes the annihilation event.

6. Conclusions

This paper presented a numerical and theoretical study of sound production by planar, axisymmetric and spherically symmetric premixed flame annihilation events. Simple chemistry simulations resolving both the flame dynamics and the acoustics, using a higher order accurate solver that was appropriate for aeroacoustic studies, was first used to examine sound production and propagation by these events. The simulations showed that annihilation events could be a significant source of sound, which was consistent with previously reported studies. The far-field sound was compared for the different annihilation configurations and for different flame thicknesses. For the planar annihilation, it was found that there was relatively little influence of flame thickness. In contrast, the far-field pressure in the axisymmetric and spherical cases were shown to exhibit a dependence on the flame thickness.

A theory was then presented that related the far-field sound to the flame annihilation by using (Dowling 1992) extended form of Lighthill's acoustic analogy. This theory retained only the heat release source term from Lighthill's equation and agreed closely with the corresponding numerical results. From these more general theoretical results, increasingly restrictive assumptions were then applied. The assumption of an infinitely thin flame propagating at constant velocity was demonstrated to be adequate for prediction of the the steady state pressure change in the planar case, but considerably underestimated the far-field pressure in the other configurations.

Inspection of the theoretical results suggested that the flame thickness and propagation velocity were significant influences in these configurations. The simulations were then used to carry out a more detailed study of the propagation velocity and heat release rates during the extinction event, showing that the behaviours could be collapsed by normalising with flame parameters. The observations were then used to hypothesize the basic dependence of far-field pressure with the Mach number, ratio of flame thickness to observer distance, and heat release parameter. These basic scalings were observed to perform well in comparison with the simulations.

The authors acknowledge the generous support of the European Centre for Research and Advanced Training in Scientific Computation (CERFACS, www.cerfacs.fr), in providing the authors with the source code for NTmix. Use of the facilities of the Victorian Partnership for Advanced Computing (VPAC) is also acknowledged.

REFERENCES

Baillot, F., Durox, D. & Demare, D. 2002 Experiments on imploding spherical flames: effects of curvature. *Proc. Combust. Inst.* **29** (2), 1453–1460.

Balachandran, R., Ayoola, B. O., Kaminski, C. F., Dowling, A. P. & Mastorakos, E. 2005 Experimental investigation of the nonlinear response of turbulent premixed flames to imposed inlet velocity oscillations. *Combust. Flame* **143** (1–2), 37–55.

Baum, M. 1994 Etude de l'allumage et de la structure des flammes turbulentes. PhD thesis, Ecole Centrale Paris.

Birbaud, A. L., Ducruix, S., Durox, D. & Candel, S. 2006 Dynamics of free jets modulated by plane acoustic waves: Part II. Numerical simulations. In *12th AIAA/CEAS Aeroacoustics Conference (27th AIAA Aeroacoustics Conference)*, Cambridge, MA, *AIAA*-2006-2670.

Bourlioux, A., Cuenot, B. & Poinsot, T. 2000 Asymptotic and numerical study of the stabilization of diffusion flames by hot gas. *Combust. Flame* **120** (1–2), 143–159.

Bradley, D., Gaskell, P. H. & Gu, X. J. 1996 Burning velocities, Markstein lengths, and flame quenching for spherical methane-air flames: a computational study. *Combust. Flame* **104** (1–2), 176–198.

Bragg, S. L. 1963 Combustion noise. *J. Inst. Fuel* **36** (264), 12–16.

Bui, T. P., Meinke, M., Schröder, W., Flemming, F., Sadiki, A. & Janicka, J. 2005 A hybrid method for combustion noise based on LES and APE. In *11th AIAA/CEAS Aeroacoustics Conference (26th AIAA Aeroacoustics Conference)*, Monterey, CA.

Bui, T. P., Schröder, W. & Meinke, M. 2008 Numerical analysis of the acoustic field of reacting flows via acoustic perturbation equations. *Comput. Fluids* **37** (9), 1157–1169.

Candel, S., Durox, D., Ducruix, S., Birbaud, A. L., Noiray, N. & Schuller, T. 2009 Flame dynamics and combustion noise: progress and challenges. *Intl J. Aeroacoust.* **8** (1 & 2), 1–56.

Candel, S., Durox, D. & Schuller, T. 2004 Flame interactions as a source of noise and combustion instabilities. In *10th AIAA/CEAS Aeroacoustics Conference, Paper 2004-2928*, pp. 1444–1454.

Candel, S., Veynante, D., Lacas, F., Maistret, E., Darabiha, N. & Poinsot, T. 1990 *Coherent Flamelet Model: Applications and Recent Extensions. Recent Advances in Combustion Modelling*. World Scientific.

Chen, C. L. & Sohrab, S. H. 1995 Upstream interactions between planar symmetric laminar methane premixed flames. *Combust. Flame* **101** (3), 360–370.

Clavin, P. & Siggia, E. D. 1991 Turbulent premixed flames and sound generation. *Combust. Sci. Technol.* **78**, 147–155.

Corjon, A. & Poinsot, T. 1995 A model to define aircraft separations due to wake vortex encounter. In *13th AIAA Applied Aerodynamics Conference. AIAA Paper* 95-1776., pp. 117–124.

Corjon, A. & Poinsot, T. 1997 Behavior of wake vortices near ground. *AIAA J.* **35** (5), 849–855.

Cuenot, B., Bedet, B. & Corjon, A. 1997 *NTMIX3D User's Guide Manual, Preliminary Version 1.0*.

Dowling, A. P. 1992 *Modern Methods in Analytical Acoustics*, chap. Thermoacoustic sources and instabilities, pp. 378–403, Springer.

Dowling, A. P. & Ffowcs Williams, J. E. 1983 *Sound and Sources of Sound*. Ellis Horwood.

Duffy, D. G. 2001 *Green's Functions with Applications*. Chapman & Hall/CRC.

Durox, D., Ducruix, S. & Candel, S. 2001 Experiments on collapsing cylindrical flames. *Combust. Flame* **125** (1–2), 982–1000.

Durox, D., Schuller, T., Noiray, N. & Candel, S. 2009 Experimental analysis of nonlinear flame transfer functions for different flame geometries. *Proc. Combust. Inst.* **32** (1), 1391–1398.

Echekki, T. & Chen, J. H. 1999 Analysis of the contribution of curvature to premixed flame propagation. *Combust. Flame* **118** (1), 308–311.

Echekki, T., Chen, J. H. & Gran, I. R. 1996 The mechanism of mutual annihilation of stoichiometric premixed methane–air flames. *Proc. Combust. Inst.* pp. 855–864.

Flemming, F., Sadiki, A. & Janicka, J. 2007 Investigation of combustion noise using a LES/CAA hybrid approach. *Proc. Combust. Inst.* **31** (2), 3189–3196.

Gibson, C. H. 1968 Fine structure of scalar fields mixed by turbulence. Part I. Zero-gradient points and minimal gradient surfaces. *Phys. Fluids* **11**, 2305–2315.

Hassan, H. A. 1974 Scaling of combustion-generated noise. *J. Fluid Mech.* **66** (3), 445–453.

Hirsch, C., Wäsle, J., Winkler, A. & Sattelmayer, T. 2007 A spectral model for the sound pressure from turbulent premixed combustion. *Proc. Combust. Inst.* **31** (1), 1435–1441.

Howe, M. S. 1998 *Acoustics of Fluid-Structure Interactions*. Cambridge University Press.

Hurle, I. R., Price, R. B., Sugden, T. M. & Thomas, A. 1968 Sound emission from open turbulent premixed flames. *Proc. R. Soc. Lond. Ser. A, Math. Phys. Sci.* **303** (1475), 409–427.

Ihme, M., Bodony, D. J. & Pitsch, H. 2006 Prediction of combustion-generated noise in non-premixed flames using large-eddy simulation. In *12th AIAA/CEAS Aeroacoustics Conference (27th AIAA Aeroacoustics Conference)*, Cambridge, Massachusetts.

Ihme, M., Pitsch, H. & Bodony, D. J. 2009 Radiation of noise in turbulent non-premixed flames. *Proc. Combust. Inst.* **32** (1), 1545–1553.

Karimi, N., Brear, M. J., Jin, S. H. & Monty, J. P. 2009 Linear and non-linear forced response of a conical, ducted, laminar premixed flame. *Combust. Flame* **156** (11), 2201–2212.

Kidin, N., Librovich, V., Macquisten, M., Roberts, J. & Vuillermoz, M. 1988 Possible acoustic source in turbulent combustion. *Dyn. Reactive Syst. Part 1: Flames* pp. 336–348.

Kidin, N., Librovich, V., Roberts, J. & Vuillermoz, M. 1984 On sound sources in turbulent combustion. *Dyn. Flames Reactive Syst.* pp. 343–355.

Kotake, S. 1975 On combustion noise related to chemical reactions. *J. Sound Vib.* **42**, 399–410.

Laverdant, A. & Thévenin, D. 2003 Interaction of a gaussian acoustic wave with a turbulent premixed flame. *Combust. Flame* **134** (1–2), 11–19.

Laverdant, A. & Thévenin, D. 2005 Direct numerical simulation of a gaussian acoustic wave interaction with a turbulent premixed flame. *Comptes Rendus-Mécanique* **333** (1), 29–37.

Lieuwen, T. 2003 Modeling premixed combustion-acoustic wave interactions: A review. *J. Propul. Power* **19** (5), 765–781.

Lieuwen, T., Mohan, S. & Rajaram, R. 2006 Acoustic radiation from weakly wrinkled premixed flames. *Combust. Flame* **144** (1–2), 360–369.

Lieuwen, T. & Yang, V., (Ed.) 2006 *Combustion Instabilities in Gas Turbine Engines: Operational Experience, Fundamental Mechanisms and Modeling*, vol. 210. Progress in Astronautics and Aeronautics, AIAA.

Lighthill, M. J. 1951 On sound generation aerodynamically I. General Theory. *Proc. R. Soc. Lond.* **211**, 564–587.

Lu, Z. & Ghosal, S. 2003 A similarity solution describing the collision of two planar premixed flames. *Combust. Theory Model.* **7** (4), 645–652.

Lu, Z. & Ghosal, S. 2004 Flame holes and flame disks on the surface of a diffusion flame. *J. Fluid Mech.* **513**, 287–307.

Miyauchi, T., Tanahashi, M. & Li, Y. 2001 Mechanism and prediction of sound generation in reacting mixing layers. In *2nd Symposium on Smart Control of Turbulence*, University of Tokyo, Japan.

Mohseni, K. & Colonius, T. 2000 Numerical treatment of polar coordinate singularities. *J. Comput. Phys.* **157** (2), 787–795.

Najafi-Yazdi, A., Lew, P. T. & Mongeau, L. 2010 Direct numerical simulation of sound radiation by a diffusion flame in a planar shear layer. In *16th AIAA/CEAS Aeroacoustics Conference*, pp. 441–458.

Pantano, C. & Pullin, D. I. 2003 On the dynamics of the collapse of a diffusion-flame hole. *J. Fluid Mech.* **480**, 311–332.

Petrov, C. A. & Ghoniem, A. F. 1998 Dynamics and structure of interacting nonpremixed flames. *Combust. Flame* **115** (1–2), 180–194.

Poinsot, T. & Veynante, D. 2005 *Theoretical and Numerical Combustion*. RT Edwards, Inc.

Poinsot, T. J. & Lele, S. K. 1992 Boundary conditions for direct simulations of compressible viscous flows. *J. Comput. Phys.* **101** (1), 104–129.

Schuller, T., Durox, D. & Candel, S. 2002 Dynamics of and noise radiated by a perturbed impinging premixed jet flame. *Combust. Flame* **128** (1–2), 88–110.

Schwarz, A. & Janicka, J., (Ed.) 2009 *Combustion Noise*. Springer.

Shalaby, H., Laverdant, A. & Thévenin, D. 2009 Direct numerical simulation of a realistic acoustic wave interacting with a premixed flame. *Proc. Combust. Inst.* **32** (1), 1473–1480.

Sivashinsky, G. I. 1974 On a converging spherical flame front. *Intl J. Heat Mass Transfer* **17**, 1499–1506.

Smith, T. J. B. & Kilham, J. K. 1963 Noise generation by open turbulent flames. *J. Acoust. Soc. Am.* **35**, 715–724.

Strahle, W. C. 1971 On combustion generated noise. *J. Fluid Mech.* **49** (2), 399–414.

Strahle, W. C. 1978 Combustion noise. *Prog. Energy Combust. Sci.* **4**, 157–176.

Strahle, W. C. 1985 A more modern theory of combustion noise. In *Recent Advances in Aerospace Sciences*, pp. 103–114. Plenum Press.

Sun, C. J. & Law, C. K. 1998 On the consumption of fuel pockets via inwardly propagating flames. *Proc. Combust. Inst.* **27**, 963–970.

Talei, M. 2011 Sound generation by combusting and non-combusting, low Mach number flows. PhD thesis, Department of Mechanical Engineering, The University of Melbourne.

Tanahashi, M., Tsukinari, S., Saitoh, T., Miyauchi, T., Gyung-min, C., Ikame, M., Kishi, T., Harumi, K. & Hiraoka, K. 2002 On the sound generation and its controls in turbulent combustion field. In *3rd Symposium on Smart Control of Turbulence*, University of Tokyo, Japan.

Thomas, A. & Williams, G. T. 1966 Flame noise: sound emission from spark-ignited bubbles of combustible gas. *Proc. R. Soc. Lond. Ser.* A*, Math. Phys. Sci.* **294** (1439), 449–466.

Truffaut, J. M., Searby, G. & Boyer, L. 1998 Sound emission by non-isomolar combustion at low mach numbers. *Combust. Theory Model.* **2** (4), 423–428.

Wichman, I. S. & Vance, R. 1997 A study of one-dimensional laminar premixed flame annihilation. *Combust. Flame* **110** (4), 508–523.

Zhao, W. & Frankel, S. H. 2001 Numerical simulations of sound radiated from an axisymmetric premixed reacting jet. *Phys. Fluids* **13**, 2671–2681.